Refractive index estimation in biological tissues by quantitative phase imaging

Carlos Cairós [a,*], Ricardo Oliva-García [b], Gabriela Siverio [a], Juan Manuel Trujillo-Sevilla [b], José Manuel Rodríguez-Ramos [b], Ángel Acebes [a,**]

[a] Department of Basic Medical Sciences, Institute of Biomedical Technologies, University of La Laguna (ULL), Tenerife, 38200, Spain
[b] Wooptix S.L., Avda Trinidad 61 Planta 7, La Laguna, Tenerife, 38205, Spain

A B S T R A C T

The refractive index (RI) of biological tissues represents a relevant optical property that correlates with intrinsic factors such as dry mass or water content, providing valuable information about tissue composition. First, we review available methods to measure the RI in biological tissues, making special emphasis on quantitative phase imaging (QPI) and its ability to obtain RI maps as well as tri-dimensional projections of transparent samples at diffraction-limited resolution. Second, we propose a simple, general QPI method to estimate the RI of complex materials without prior knowledge of sample thickness. Here we have tested several samples in various immersion media with different refractive indices (RIs) to use the lineal relation between the optical path difference (OPD) and the RI of the medium. Least squares regression operates to simultaneously determine the RI and the thickness with diffraction-limited resolution and nanometric transversal sensitivity. Our findings categorize a set of immersion media covering a good RI range, identify possible error sources and uncover the applicability of the QPI method, paving the way to its use on heterogeneous biological tissues.

1. Introduction

Refractive index (RI) is a physical magnitude defined as the ratio between the speed of light in a medium with respect to vacuum. The refractive index of an optically heterogeneous sample can vary in parallel and perpendicular lines with respect to the axis of the microscope. In complex biological tissues or cell structures the refractive index can differ in any of the spatial dimensions [1]. RI is defined as a complex magnitude with the real part reflecting scattering effects and the complex part related to absorption effects [2]. In phase microscopy, as the samples are transparent and are therefore considered not absorbent, the imaginary part of the RI can be, in a first approximation, neglected. Throughout this work, we will refer to RI as the real part of the refractive index. As a phase object in the initial approach, it can be assumed that the refractive index is uniform throughout the thickness of the sample, with variations occurring only in the plane perpendicular to the direction of the incident light.

Currently several techniques employed to determine the refractive index of a material are classified according to data acquisition as one-dimensional (1D), two-dimensional (2D) or three-dimensional (3D). Classical methods as total internal reflection (TIR) [3], Abbe refractometry [4], or ellipsometry [5] belong to the first group, as they obtain a single RI value for a relatively large illuminated area of sample, generally mm^2. These techniques have reached high accuracy and robustness with the development of improved commercial instruments but, in general, they are limited to flat, small-size, homogeneous materials, with no surface roughness [1]. In addition, material samples need to be mounted - and therefore compressed-between glass surfaces, a fact that notably affects measurement accuracy. For non-homogeneous samples, the refractive index obtained using these techniques corresponds to an effective refractive index, which is a complex combination of the various paths that light may travel through the sample and the interactions that occur at each of the interfaces where a refractive change takes place. The effective refractive index is largely dependent on the illuminated area of the sample and the size and distribution of heterogeneities within the sample [6,7]. There are several articles that review the application of this methods on biological tissues, their limitations and advantages [8,9].

---

* Corresponding author.
** Corresponding author.
E-mail addresses: ccairosb@ull.edu.es (C. Cairós), aacebesv@ull.edu.es (Á. Acebes).

In the second category, Quantitative Phase Imaging (QPI) methods provide two-dimensional (2D) data. QPI refers to a collection of microscopy techniques that recover the phase delay of the wavefront to generate Optical Path Difference (OPD) maps, the magnitude measured in QPI, an effective difference in the path that travels the light between 2 media of different RI. These maps can provide diffraction limited resolution in X,Y plane (perpendicular to direction of light) and nanometer-level sensitivity in Z-axis (in the direction of the light) [10]. These methods provide information on how the refractive indices are distributed in the X and Y directions, but only when the heterogeneities of the sample are larger than the optical resolution of the instrument. Most biological organelles and tissues fulfil this condition when the instrument is operated at resolutions close to the diffraction limit. It should be emphasized that these techniques are unable to reveal differences in refractive indices along the Z-axis, which is perpendicular to the sample plane. For QPI methods to be applicable, it is essential to assume a constant RI along the light path on the Z-axis. Phase samples, which are typically thin and transparent with no light scattering or absorption effects, generally comply with this requirement, but samples showing substantial variances from any of these factors can cause inaccuracies in QPI measurements. QPI methods have been divided into 2 principal groups, interferometric, involving the use of a laser, and non-interferometric, that avoid the use of the laser, employing different approaches, most of them computational (i.e., computing a set of intensity images) [11,12]. The field of research and the number of versions of these techniques has grown exponentially in the last decade, widening the range of applications and the possibilities to utilize them in different scenarios [10,13–15].

Several approaches have been focused on the application of QPI to RI measurement. It is not our aim here to perform an extensive reviewing of the QPI literature, but to provide instead an in-depth analysis of the QPI methods as well as the strengths, weaknesses, and trade-offs between them. The methods can be classified into two main groups [16], those that rely on pre-existing or in-situ information about the sample thickness or impose a specific thickness, for example, by enclosing the sample in a confined space with a known thickness and applying enough pressure to guarantee that the sample thickness aligns with the selected container [17–19]. On the other hand, there are methods that simultaneously determine RI and thickness by making multiple measurements, either using varying spatial coordinates, wavelengths, or, as in our case, immersion liquids [20–22]. The accuracy of the "*knowledge of thickness*" methods will be mainly dependent on the precision of the technique applied to measure sample thickness, which in many cases limits the application range of the procedure to micrometer size layers. Thus, if the sample has a very heterogeneous thickness profile, it will be necessary to apply techniques such as Atomic Force Microcospy (AFM) to characterize the sample. The simultaneous determination of sample thickness and RI changes are crucial data facing complex heterogeneous samples such as biological tissues. Wavelength and temperature shifting approaches were suggested already in 1954 by Faust [23], with the advent of interferometric techniques. Improvement in instruments and computational power make wavelength shifting methods, as those shown by Song and collaborators [17], very promising, as they are fast and reproducible with minimum sample manipulation and can be implemented in most QPI versions. Nevertheless, to date there are not any commercially available instruments and, from a technical perspective, additionally wavelength shift might induce defocus artifacts on the measurement. Due to all these facts, further research on these methods is needed prior to their widespread use in biological laboratories.

Finally, with respect to 3D techniques, tomography, based in QPI or not, will yield 3D maps of RI distribution, measuring RI changes in the three directions of the space [18]. 3D accuracy will depend on Z scanning and X, Y resolution, and it is limited to static processes due to their long scanning time [21,24]. Tomography techniques will yield crucial data on heterogeneous solid tissues. However, these 3D data will need to be carefully cross-checked with results obtained by 1D and 2D methods

previously to its standardization.

Taken all this information together, it appears imperative the development of reference methods to be applied in different laboratories in the simplest manner, without demanding a great technological effort, to create reliable databases of the largest possible number of complex biological cells and tissues. This will undoubtedly help to increase our knowledge of heterogeneous biological samples and will have a deep impact on improving the diagnosis of certain diseases and our understanding of disease evolution among others.

In this work we propose a simple method, based on Yagoda et al. [20] and adapted to benefit from QPI characteristics, to estimate the RI of complex materials without previous knowledge of sample thickness. This modified method comprises the immersion of the sample in liquids with different RI to use the lineal relation between OPD, the RI of the medium n_{medium} and the minimum least squares regression to simultaneously determine sample thickness and RI with diffraction-limited resolution and nanometric transversal sensitivity for specific regions of the image. These specific regions can be selected thanks to shape characteristics that have been revealed in intensity images or 2D OPD maps. In this work, we have tested different liquids over a variety of samples. Our analysis have prompted us to recommend different liquids to work with samples of different nature in a good variety of RI intervals, discussing their applicability and also possible error sources.

2. Material and methods

2.1. QPI method

QPI is a set of techniques divided in two principal groups: interferometric and non-interferometric. Our laboratory has a previous broad expertise in the development of wavefront sensors in the fields of silicone metrology and ophthalmology [25,26]. We work in non-interferometric approaches based on defocus, avoiding lasers, by capturing two images symmetrically displaced from the focal point, illuminated by an incoherent but collimated light source.

The most common reconstruction algorithm on quantitative phase microscopy is based on the transport of intensity equation (TIE) that describes the relationship between intensity and phase distribution of a wave. Its application in microscopy has been intensively described and tested in the last decade, highlighting its ease of implementation, stability against vibration, high signal to noise ratio (SNR) and flexibility in the choice of illumination source [27].

We have developed our own algorithm, based on geometrical optics, to obtain the OPD, using first order derivative, unlike classical TIE which is based on second order derivatives, as described previously in Bonaque et al. [26]. This approach is robust to noise as it accounts for the variation in the first derivative. By avoiding the second derivative it is also more sensitive to slow frequency changes. This algorithm has been successfully used in application in metrology [25] and ophthalmology [26].

The following equations illustrate the algorithm behavior and how to obtain the phase from the two images.

$$V\big(H_{y,\alpha}\big)(x) = \int_0^x H(x, tan(\alpha)x + y)\, for \begin{cases} x \in [0, \infty) \\ \forall y \in [0, \infty) \\ \forall \alpha \in [-\pi/2, \pi/2) \end{cases} \quad \text{(eq. 1)}$$

H(x,y) is a continuous bidimensional function described for positive values **x,y** and with positive numbers, and **V** the auxiliary transformation of **H**. The factor **α** is a variable of **k** discrete angles distributed in the interval [-π/2, π/2], defining a line with **y** origin and angular separation from the **x** axis equal to **α**.

Another auxiliary function represents the abscissa axis between two unidimensional continuous functions represented by f(x) and g(x) defined for positive values of x, represented here as *D,* described in eq. (2).

$$D(f,g)(x) = argmin_x(f(x) - y) - argmin_x(g(x) - y); \ y \in [0, \infty) \qquad (eq.2)$$

Captured images called I_1 and I_2 are separate intensity maps, and then eq. (3) is applied to recover the phase with our method.

$$\varphi_h(x,y) = \frac{1}{k} \sum_{\alpha=-\frac{\pi}{2}}^{\alpha=\frac{\pi}{2}} cos(\alpha) D\left(V\left(I_{1(y,\alpha)}\right), V\left(I_{2(y,\alpha)}\right)\right)(x)$$

$$\varphi_v(x,y) = \frac{1}{k} \sum_{\alpha=-\frac{\pi}{2}}^{\alpha=\frac{\pi}{2}} sen(\alpha) D\left(V\left(I_{1(y,\alpha)}\right), V\left(I_{2(y,\alpha)}\right)\right)(x) \qquad (eq.3)$$

To convert the φ_o where o means the orientation to real units it is necessary to apply a factor represented in equation (4), the pixel size must be considered.

$$\varphi_{io} = \varphi_i \frac{s^2}{2\Delta z} \qquad (eq. 4)$$

A numerical integration of both gradients is needed to obtain the phase maps. This algorithm has been successfully applied in metrology [25] and ophthalmology [26].

2.2. Experimental setup

The experimental setup was designed to use the microscope advantages and its own optics, a light collimator and a CCD camera coupled to the microscope (Fig. 1a). This setup could be implemented in any biological laboratory with minimum effort, although we emphasize that it is a method that works with any QPI technique generating OPD maps. In turn, Fig. 1b and c shows images of the set up used to obtain the RI: an Olympus CKX-53 inverted microscopy as optical system and a ZWO camera as the detector to capture intensity images using a blue led in 470 nm wavelength adapted to collimate the light. We have coupled a motor to the fine focus knob of the microscope. As a result, every step of the motor corresponds to 0,05 μm displacement of the microscope objective. We consider this level of precision to be sufficient, as the

range of defocus distances in our experiments will vary between 10 and 20 μm. The camera is connected to a Windows 10 PC with an i5 CPU and 8 GB RAM and the PC is used to control the motor movement, camera capture and algorithm processing. The stepper takes along 1 s to move precisely, the exposure time should be added, having a processing time of around 2 s using python developed algorithms. With the simplest possible experimental setup, we can use our QPI algorithm to measure OPD with an accuracy of 7 nm. The lateral resolution of the microscope depends on the objective used and the selected propagation distance. Specifically, for the 10× objective, the final optical resolution was approximately 1,1 μm, while for the 40× objective, it was approximately 410 nm.

2.3. Samples

We have conducted experiments on different phase object samples to demonstrate the efficacy of the proposed methods for estimating the RI of materials of different nature.

2.3.1. Standard calibration samples

We have used a commercially available phase target provided by Benchmark Technologies (Lynnfield, USA), that has different elements, as USAF target or Siemens focus star with a well-characterized OPL ranging from 50 to 350 nm height and built in a transparent polymer of refractive index 1,51. The height of the elements was validated by AFM measurements by provider, and the actual values, used during this work, are, 53,9, 107,1, 160,5, 208,9 nm. The microlens array was purchased from SUSS MicroOptics SA (Hauterive, Switzerland), consisting of a $10*10 \ mm^2$ glass with an array of 100 μm of diameter and 2,5 μm maximum height. The refractive index of the glass is 1,457.

2.3.2. Immersion media

Ethanol, isopropanol, glycerol, silicone oil and castor oil were purchased from Sigma-Aldrich, quality absolute for analysis, purity >99%. Opti-Prep was obtained from Sigma-Aldrich (Germany) as a 60% w/v
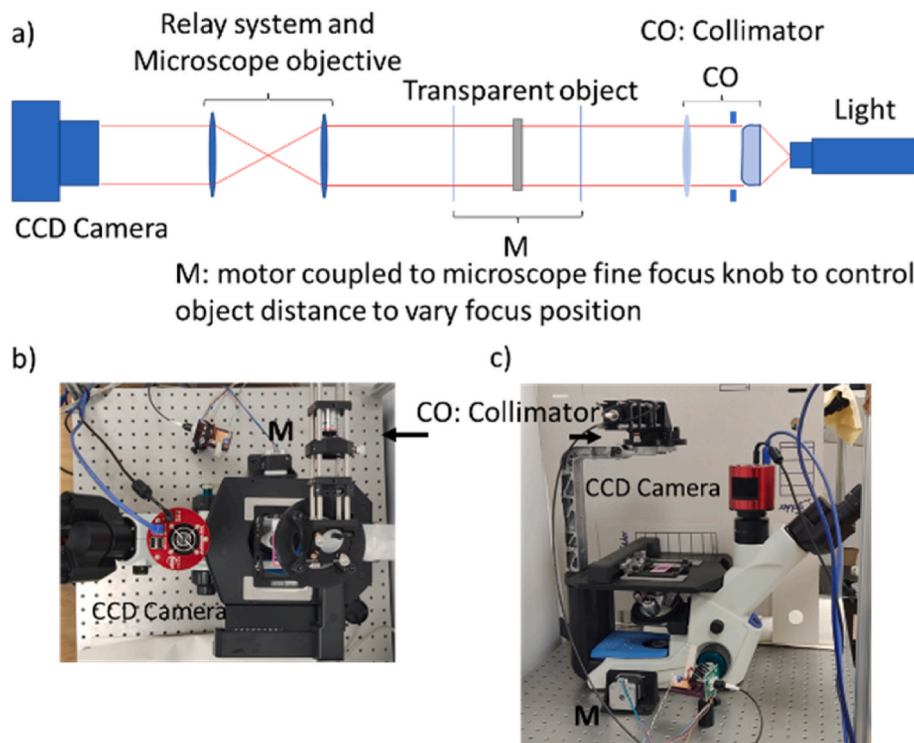
Fig. 1. Experimental set-up of our QPI system. a) Schematic description of the QPI system, b) Top view showing collimator and motor on side knob, c) The lateral view highlights the simplicity by which our system can be coupled to any routine biological microscope.

commercial solution of Iodixanol.

2.3.3. Biological samples slide preparation

The onion epidermis samples were prepared from fresh rooted onions (*Allium cepa*) that were collected from local market only 24 h after harvesting. All selected samples were obtaining from the third epidermis layer of the onion. Epidermis pieces were carefully cut and deposited in the selected Iodixanol solution prior to a microscope slide and cover with a droplet of solution. Images were captured 30 min after slide preparation, using 10× objective with a resolution of 1,1 μm. Samples from dissected *Drosophila* larvae were prepared following this procedure: Young 3rd-instar larvae were longitudinally opened with scissors (Vannas spring scissors, Fine Science Tools, catalog number: 15000-00) on a solid surface (SYLGARD 184 Silicone Elastomer Kit, Dow, USA) by having their cuticle cut near the mouth hooks and the larvae spiracles using fine pins (Auzoux Laboratories, France). The internal organs were carefully removed to enhance the exposure of the larval CNS and PNS, body walls and the trachea, the larval respiratory system. Larvae (n = 30) were directly dissected in each corresponding iodixanol solutions (15 and 45% w/v iodixanol solutions) and mounted in a glass slide containing two 20 mm × 20 mm coverslips in each side, creating a small space slightly less than the width of the open larvae between the slide and the coverslip. This avoids sample crushing and damage of larval structures. The optical resolution of the microscope was 1,1 μm and 410 nm, for measurements made using 10x and 40× objectives, respectively.

2.4. Refractive index estimation method

In our proposed methodology we aim to quantify the RI of specific regions within biological tissues by using the spatial distribution of OPD on the plane orthogonal to the light propagation axis (Image plane) obtained through QPI combined with previous knowledge of the sample and/or statistics calculations.

This approach relies on the linear correlation that can be established, under specific conditions, between the OPD and the product of the sample thickness by the gradient of the refractive index. Equation (5) shows the linear relation [28], general for QPI methods, independently of the theoretical approach, that can be expressed as equation (6) if convenient. This equation derives from the relation between intensity and phase, the transport of intensity equation, and assumptions must be done to arrive to equation (5). In the context of paraxial approximation, those assumptions include light rays traveling at small angles relative to the optical axis, gradually varying field distribution along the propagation direction, a uniform medium with a constant **RI**, and minimal,

smooth phase variations without abrupt changes.

$$OPD = t * \Delta n = t * \left(n_{sample} - n_{medium} \right) \tag{eq.5}$$

$$OPD = t * n_{sample} - t * n_{medium} \tag{eq.6}$$

If thickness, t, and the RI of the sample, n_{sample}, are kept constant, by simply varying the RI of the immersion medium, a straight line is obtained by linear regression, where the slope is the thickness and the intersection with the x-axis represents the RI of the sample multiplied by the thickness. This method was suggested, already in 1956 by Yagoda et al., in the book Physical techniques in biological research [20], but using phase microscopy and a qualitative RI estimation. With advances in computational techniques, and the development of QPI, this method has become quantitative, as QPI validates equations (1) and (2), under certain simplifications or restrictions previously mentioned, which we must ensure our system fulfils.

Fig. 2 illustrates a schematic representation of how the technique can be employed in an onion epidermis cell exemplification, demonstrating the underlying physical principles of the method and the linear correlation that enables its implementation.

The method issued by Bélanger et al. [29] measures a single sample, exposed to two liquid concentrations with osmolarities similar to that of the sample under study (cultured neurons in a perfusion chamber) registered by a interferometric QPI technique working in video mode. We believe that this type of approach will lead to a better understanding of a specific sample, obtaining a RI for each region of interest. In this case they have obtained the RI for this specific sample instead of an average refractive index of the tissue. However, the method has some drawbacks related with the complications derived from expose the same sample to different immersion liquids.

The novelty of our method relies in the fact that it is not necessary to expose the same sample to different immersion liquids. We take separate samples, in which there are repeating elements that can be assumed to have the same thickness and RI, i.e., cell nuclei or individual organelles. We identify these elements by using OPD maps and statistically study them to eliminate potential outliers, in this case using the Z-score indicator assuming a normal distribution. Once the characteristic OPD values for each element under study are selected, the arithmetic mean of OPD is calculated for each of the immersion media used. The obtained OPD values are plotted against the RI of the medium and from the regression line, the average RI of the sample and the average thickness are obtained using Eq. (6). The flowchart of the method with the selection of the characteristic regions, the equations for OPD selection and the discrimination of outliers by using the Z-score together with
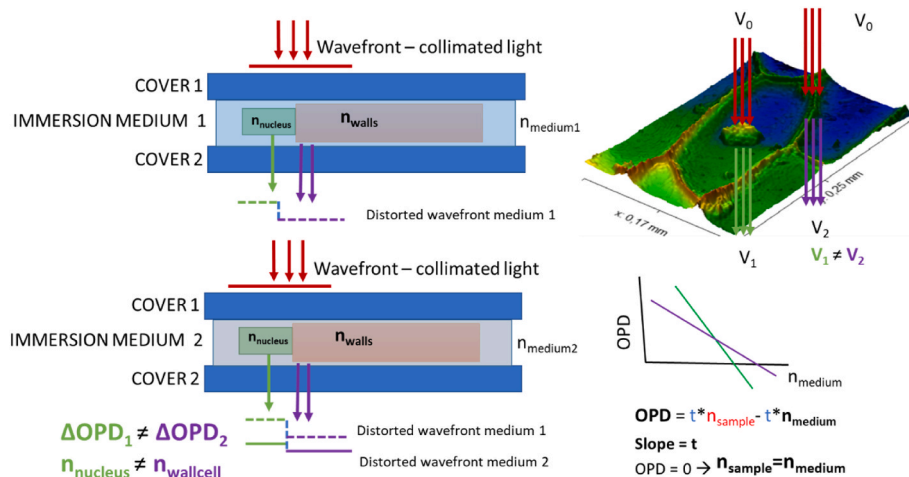

Fig. 2. Schematic representations of the physics fundamentals principles of the RI estimation method. The distortion of the wavefront changes from different RI media in a different proportion when light passes through parts of the sample with different RI. The linear relationship that can be stablish will reflect this fact with changes in slope and in the intercepts of the x and y-axes.

sampling criteria have been all depicted in Fig. 3. In the variables described in the flowchart, M represents the number of media with different refractive indices to be evaluated. In our case, this variable has a value of 5. N is the number of samples with similar characteristics to evaluate the IR, and this number depends on the number of particles presented in each image, which was between 10 and 50.

Our approach does not yield a highly precise RI for a specific part of the sample (although this precision depends on the chosen QPI technique and the number of replicates together with other technical factors as SNR or quality of the illumination). Indeed, there are alternative methods in the literature providing greater precision [8]. However, our method does offer an average RI, which serves as an objective value for unambiguously identifying distinct RI regions in situations or areas where more accurate techniques may be challenging to apply.

In this context, the values derived from our approach can work as an initial point for iterative processes or as a preliminary input to validate theoretical models. This is possible because our method enables the acquisition of RI in numerous distinctive regions of the same sample, which can then be compared to effective RI obtained using one-dimensional (1D) techniques.

3. Results and discussion

First, we aimed to validate the feasibility of our method in inorganic materials, using the commercial phase target and a microlens array. These samples do not present the sample-immersion fluid interaction problems which may affect biological samples such as chemical interaction, surface tension or osmotic diffusion.

The estimation process of RI was tested on a microlens array (Fig. 4). A single microlens has 100 μm of diameter and 2,5 μm of curvature diameter or height. The material of the array is fused silica gel with a RI of 1,457 (as indicated by the manufacturer). Fig. 4a shows the QPI maps

of the microlens array immersed in a battery of selected liquids: Water, Ethanol, Isopropanol, Silicone oil and Castor oil. Fig. 4b and c are representations of the QPI maps showing the quality of reconstruction and an example of the cross-section lines collected to obtain the OPD of each microlens. The plot of the average OPD against the refractive index of each immersion solution is shown in Fig. 4d. A least-squares regression line is fitted with R^2 value higher than 0,99 and from the equation of the line, the average refractive index and average thickness values are estimated. We obtained a RI of 1,461 and a thickness of 2,552 μm, data that were posteriorly verified with the values indicated by the manufacturer.

In turn, Fig. 5 shows an example of the USAF phase map on the 100 nm height calibration target. 3D projections are presented in Fig. 5b and c where we show an example of the cross-section lines used to obtain the average OPD, of a minimum of 30 measurement (10 images, three lines), for each height and each immersion medium. Values are represented as shown in Fig. 5d and regression lines were fit for each height with R^2 values higher than 0,99. We obtained the thickness, or step size, from the equation of each regression line, directly on the slope, and the estimated RI of the material from the cut with the X-axis, when the OPD tends to 0. Our estimated RIs were 1,512, 1,514, 1,508, 1,519 and the corresponding estimated heights were 208, 157, 108, and 63 nm in agreement with reference values provided by the QPI calibration target manufacturer.

Next, we moved to biological samples by estimating the RI of onion epidermis cell walls and nuclei immersed in iodixanol water solutions (Fig. 6). The selection of immersion media, a trivial question in inactive inorganic materials, becomes relevant when our method is applied on biological samples. Surface tension effects as hydrophobicity and osmolarity through biological cell membranes play a crucial role and deserve a careful consideration. Iodixanol solutions have been recommended as a non-toxic and non-disturbing immersion media for RI
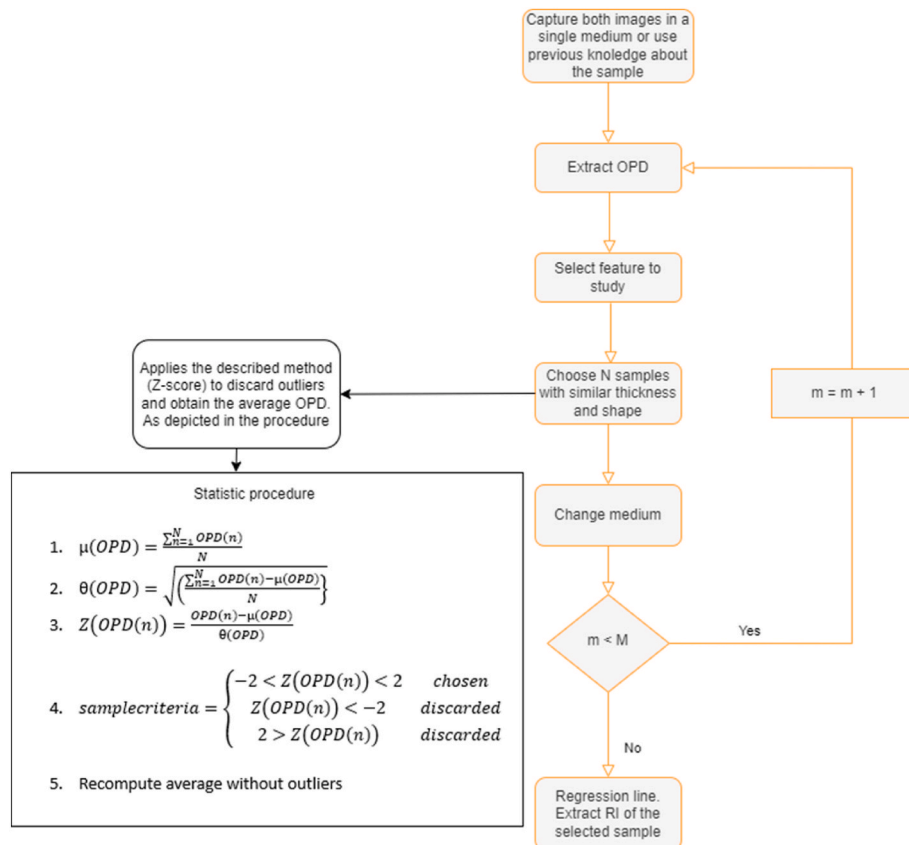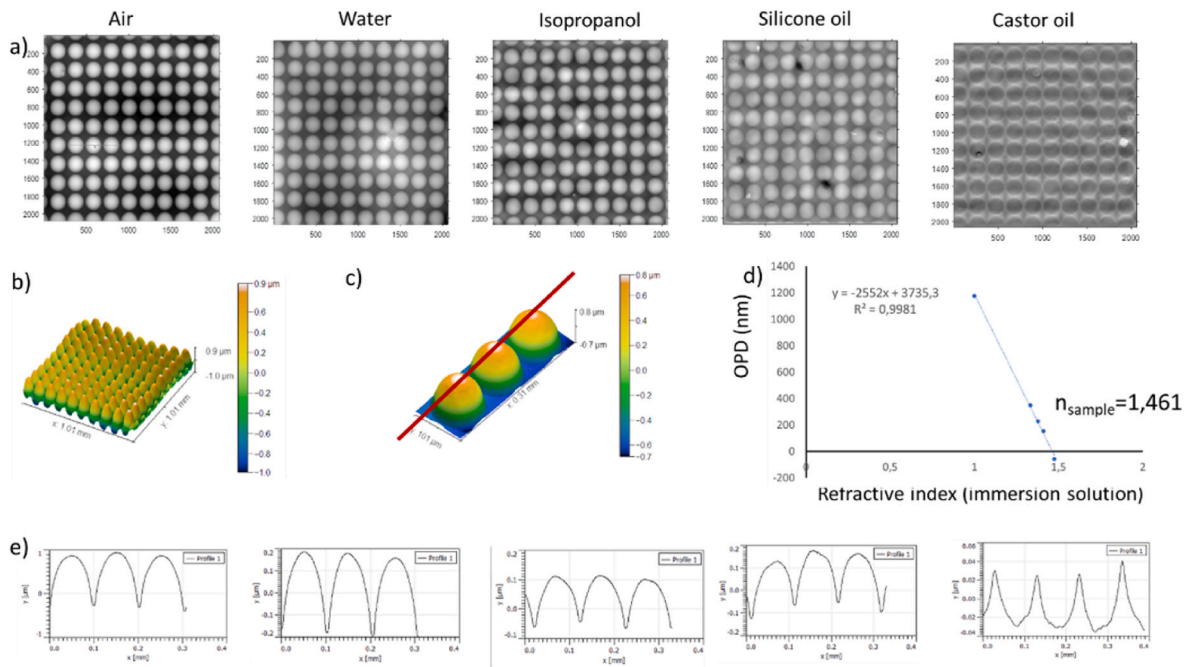

Fig. 3. Flowchart of the method for estimating the RI of selected regions, showing criteria for OPD selection within each region of interest as well as outlier exclusion.

Fig. 4. Results of the refractive index estimation of microlens array material. a) Phase maps of the microlens array immersed in different liquids (from right to left): air, water, isopropanol, silicone oil, castor oil. b) 3D projection of the phase map corresponding to air. c) Example of cross-section of three lenses. d) RI obtained after applying procedure. e) Examples of profiles used to obtain average OPD for each immersion liquid.
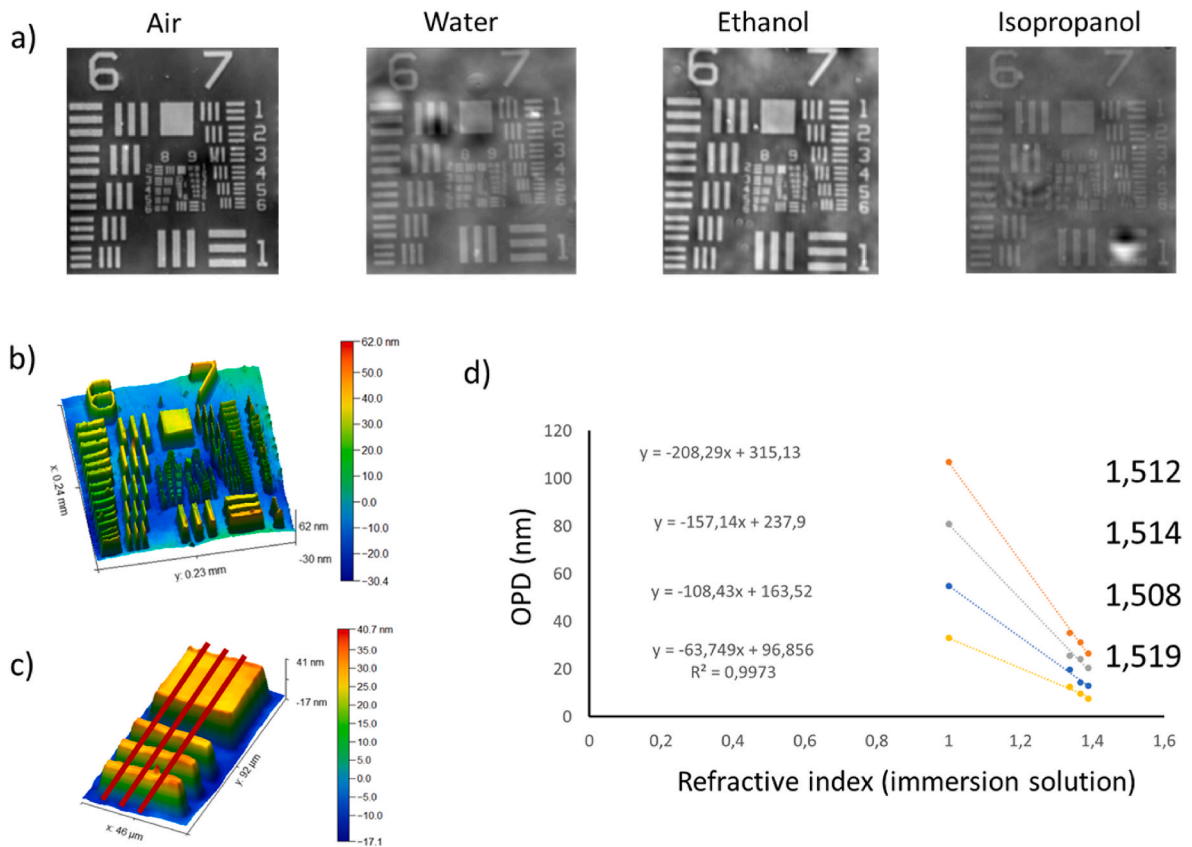
Fig. 5. Experiment performed over a commercial calibration target. The method was applied over the USAF on 4 different heights, 50 nm, 100 nm, 150 nm, 200 nm. a) OPD maps in immersion media, air, water, ethanol, isopropanol. b) and c) 3D projection of OPD map of USAF 100 nm in air. d) regression lines for four heights of the USAF, from up to down: 208, 157, 108, and 63 nm and the corresponding RI 1.512, 1.514, 1.508, 1,519.
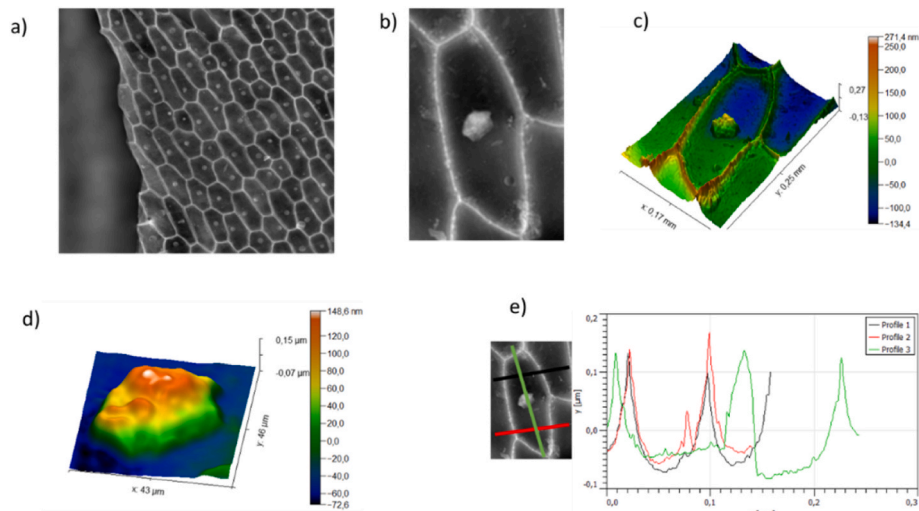
Fig. 6. Phase map of an epidermis layer on onion obtained by QPI. a) Full field of view QPI image of onion epidermis in Iodixanol 15% w/v. b) Detail of one epidermal cell with well-defined cell walls and nucleus. c) 3D projections of the QPI map. D) Detail of the nucleus showing its irregular surface. e) An example of the cross-section profiles used to obtain OPD heights of cell wall and nucleus.

matching [30]. Its toxicity and osmolarity have been very well established, as it is a common density gradient medium designed for *in vitro* isolation of biological particles, fractionation, and separation of cells [31]. Therefore, the selection of this immersion medium is clearly recommended for biological samples if the RI range suits the needs of the experiment, i.e., whether the estimated RI is relatively close to Iodixanol. A representative example of a quantitative phase map of onion epidermis immersed in a 15% w/v Iodixanol/water mixture is shown in Fig. 6a. A detailed cell is zoomed in **6b**, whereas **6c and 6d** are 3D reconstructions of the cells using OPD values. In Fig. 6e we show an example of the cross-sections we utilize to obtain wall and nucleus OPD height.

We estimated the RI of cell walls and cell nucleus in onion epidermis (Fig. 7). Fig. 7a indicates a set of phase maps for each immersion liquid. We collected the data for each immersion medium and applied the statistical criterion to obtain the OPD for each of these media, as described in the flowchart (Fig. 3), both for, the nucleus, if visible in this cell, and the cell walls, analyzing in each case more than 45 cells and three profiles for cell (such as those exemplified in 6**e**). After discarding outliers, we selected about 20 OPDs for each immersion medium and cell part, nucleus or cell wall. Finally, we calculated an average OPD for the nucleus and walls for each immersion medium and represented each OPD versus the refractive index of the immersion medium.

In Fig. 7b and **c** we display the regression lines with corresponding equations for both cell parts. As shown in **7b**, the average RI of the cell walls falls inside the iodixanol/water solutions RI range-with negative and positive values of OPD- and the RI of the cell walls can be directly extracted from the abscissa axis cut. In the case of cell nucleus, the RI is higher and must therefore be extrapolated from the regression line equation. Considering the iodixanol osmolarity, the contact of the liquid with the nuclei is guaranteed by waiting an appropriate time (10 min) between the sample preparation and the image acquisition.
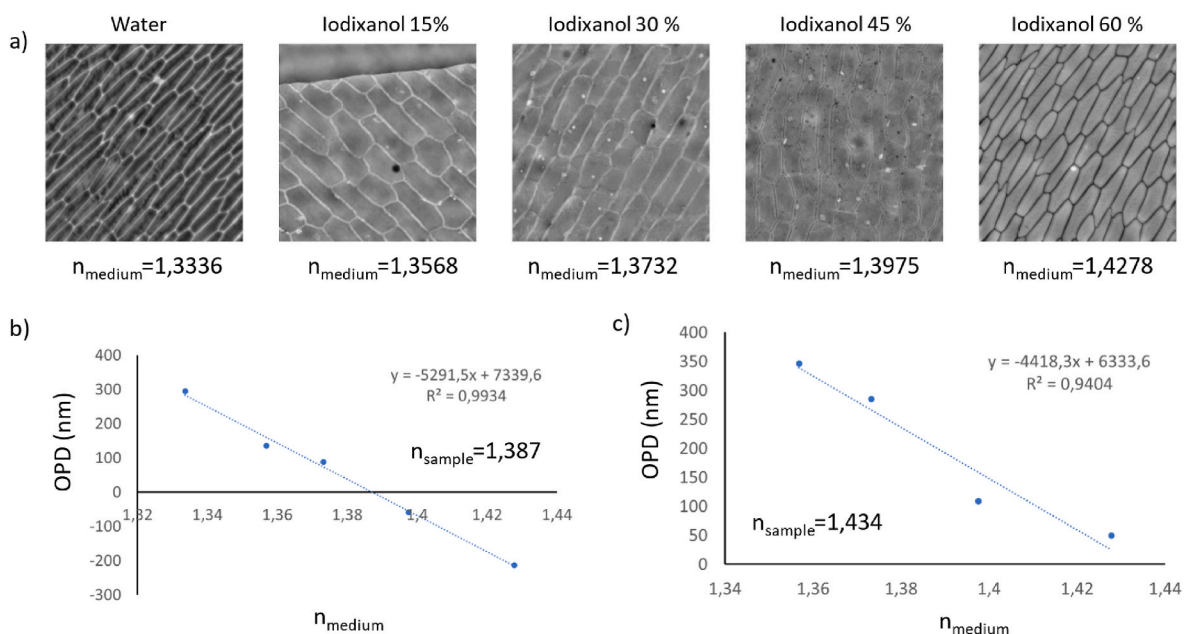

Fig. 7. RI estimation of cell walls and cell nucleus from onion epidermis. a) Phase maps for the 5 concentrations of Iodixanol, b) Regression lines for both cases allow to obtain average refractive index and average cell wall height.

Our estimated RI values are 1,387 for cell walls and 1,434 for cell nucleus while the average thickness was estimated to be 5,3 μm, similar to references found in literature [32,33]. Onion epidermis cell walls RI values obtained in our method were comparable with previous reported data [34,35]. It should be noted that these values may vary significantly depending on the type of onion used, developmental stage, and other technical factors as the resolution of the optical system. Nonetheless, they are within the range of expected values. This method can be implemented with a cross-validation procedure, using the RI iteratively to obtain the cell wall heights, and checking with another technique as AFM whether average value agrees with the one obtained with this method, or correcting it if a subjective cut-off value is defined. This approach enables the estimation of the refractive index of distinct visible parts of an onion epidermal cell without the need to expose the same sample to various immersion liquids, simply by assuming some degree of uniformity among the different cells. The resulting refractive index denotes an arithmetic average of all the analyzed cells, and while it does not precisely reflect the refractive index of any individual cell, it provides an estimated value that can serve as a reference for subsequent studies.

We later asked whether QPI can be employed to face the analysis of a complex biological tissue: the dissected full body of the *Drosophila* fly larvae. This is a very irregular and heterogeneous sample containing nervous tissue (larval CNS and PNS), body wall structure and internal organs, representing a clear example of a far-from-ideal tissue to be studied with QPI, since it may present a wide scale of OPD, possibly above the quantitative limit of the technique in many areas of the image. Indeed, such a heterogeneous biological sample like this may contain opaque or highly absorbing sections giving phase values difficult to interpret and a challenge to obtain valuable information with the QPI method. However, our results demonstrates that QPI applied to a larval internal component (lipid droplets, Fig. 8) and a larval anatomical structure (larval tracheae, Fig. 9) reveal a characteristic shape that can be determined in the phase maps. More interestingly, their corresponding refractive indices can be estimated in all dissected larvae (n = 30).

As an internal component, larval lipid droplets are continuously present at all developmental stages of Drosophila providing energy and membrane components needed to boost embryonic and larval growth, metamorphosis, and adulthood. As in higher organisms, triacylglycerol represent the fly major storage lipids of lipid droplets [36]. Fig. 8 shows examples of lipid droplets distributed in larval tissue body (**8a**). The diameter and OPD height are extracted from cross-section profiles (**8b**) as well as examples of positive and negative OPD signals of lipid droplets present in 15 and 45% w/v Iodixanol solutions, respectively (**8c**). More than 12 droplets of lipids approximately 25 μm diameter were located and analyzed for each immersion solution. We studied isolated lipid droplets from the larva, which were accidently left outside the larva bodies and were isolated on the microscope slide during dissection. We observed a slight tendency to underestimate the OPD of the lipid
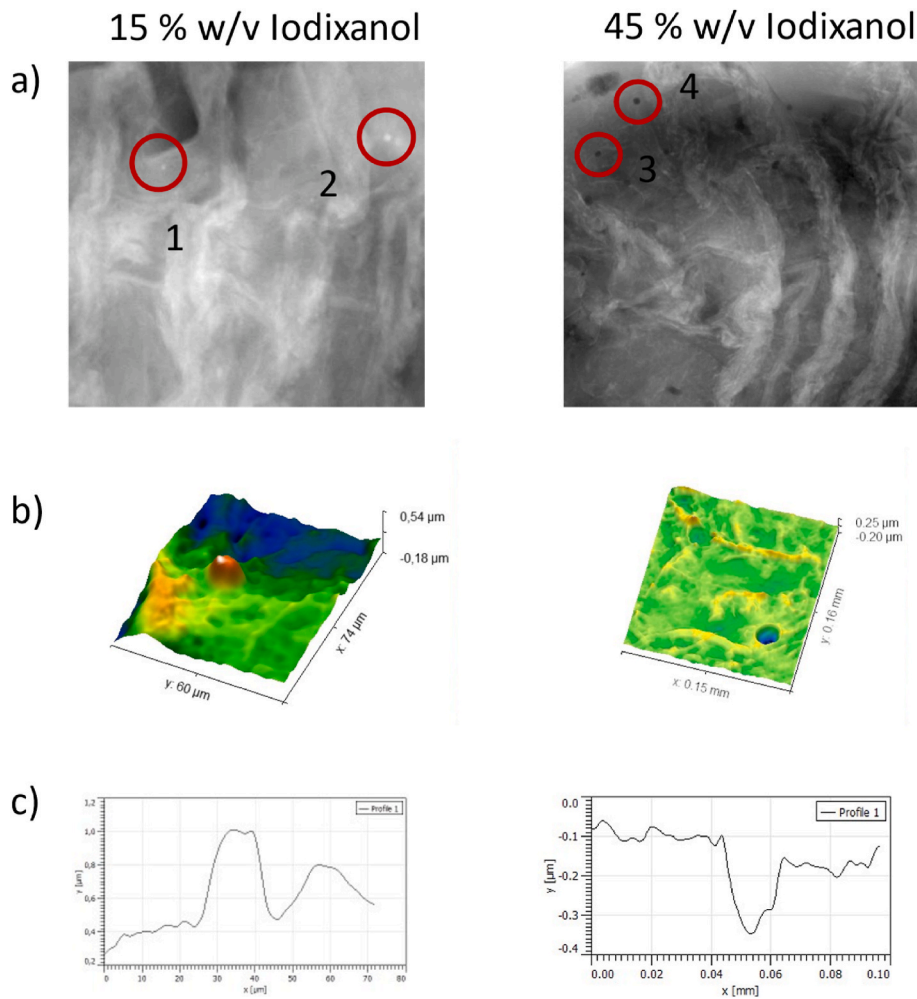
Fig. 8. Estimation of RI from Drosophila larvae lipid droplets. a) Phase maps of dissected Drosophila larval tissues showing lipid droplets (red circles) b) Cross-section profiles, c) 3D projections with lipid droplets have a RI higher than Iodixanol 15% w/v (positive values) and have a RI lower than Iodixanol 45% w/v (negative values).
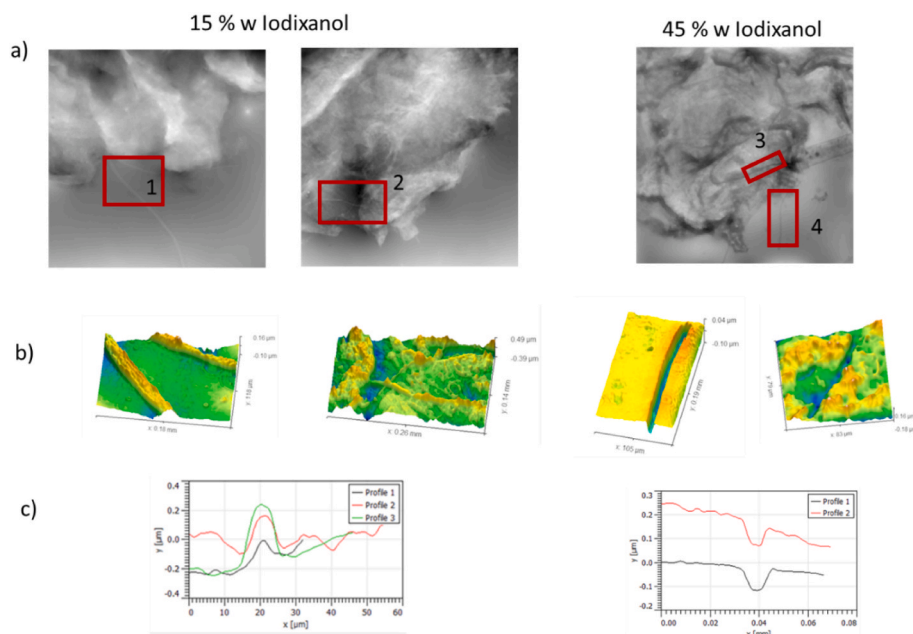
Fig. 9. Estimation of RI of tracheae from Drosophila dissected larvae. a) QPI maps for 15% w Iodixanol solution, red squares indicate selected trachea, b) 3D projection, c) Cross-section profiles of three different tracheae. d) QPI maps for 45% w/v Iodixanol solution, red squares indicate selected trachea. e) 3D projections of the tracheae selected in figure d, clearly showing negative values of OPD for this region, d) cross-section of two tracheae in 45% w/v Iodixanol.

droplets when they were inside the dissected body. This is related to light scattering in samples that do not represent an ideal phase sample and the fact that there is variation in refractive indices along the path of light. This underestimation of the value was quantified and did not exceed 10% in any case. Therefore, the assumption of a phase object is considered valid if the regression lines obtained have an R^2 greater than 90%, although it should be noted that there may be an associated error of approximately 10%.

To perform our analysis over an anatomical structure, we focused on the *Drosophila* melanogaster tracheal system. This system is composed of rigid lined tubes ramifying throughout the body and functions as the fly respiratory organ. Fig. 9 displays examples of small larval tracheae located inside the larva body or protruding from larval tissue as indicated with red squares (**9a**). For both examples, all collected data was classified from the X, Y diameter, taken from phase maps, and the more frequent size was selected to apply the method. As each trachea showed a variable diameter (**9b**), several cross-section profiles were collected for each immersion liquid sample starting from a minimum diameter of approximately 10 μm.

We finally analyzed the corresponding regression lines from lipid droplets and larval tracheae, with their respectively equations, the values of the average refractive index obtained on the abscissa axis cut and the thickness on the slope of the lines (Fig. 10). Our data indicate

that the value of average refractive index is 1,417 for lipid droplets and 1,382 for tracheae. The estimated average thickness for lipid droplets (23,9 μm) matches appropriately with the diameter of the elements calculated for X, Y coordinates, under the supposition of spherical shape. Tracheae OPD (3,54 μm) might reflect the thickness of trachea walls without air inside and collapsed into the plane of the microscope slide.

After all this detailed analysis with a battery of inorganic and organic samples as well as considering previous experiments carried out in our laboratory, we will recommend 4 different sets of immersion liquids that will cover a good range of refractive index and give versatility to act on samples of different nature (Table 1).

The technique used to measure RI will delimit the type of information obtained. 2D methods, such as QPI, provide valuable information on the distribution of RI per unit area. We would like to point out that values of RI estimated by 2D methods depend on the resolution of the intensity images and the final QPI maps. More research is needed to elucidate the correlation between RI distributions on surfaces and effective RI, as many practical effects can divert the expected average RI from the sum of single RI measurements in biological samples. These effects are related with scattering, non-uniformities, absorption, air-bubbles existence, etc. The more homogeneous and transparent a sample is, the easier it would be to stablish this relationship and to apply QPI methods. Wavelength shifting techniques [17] in a combination with
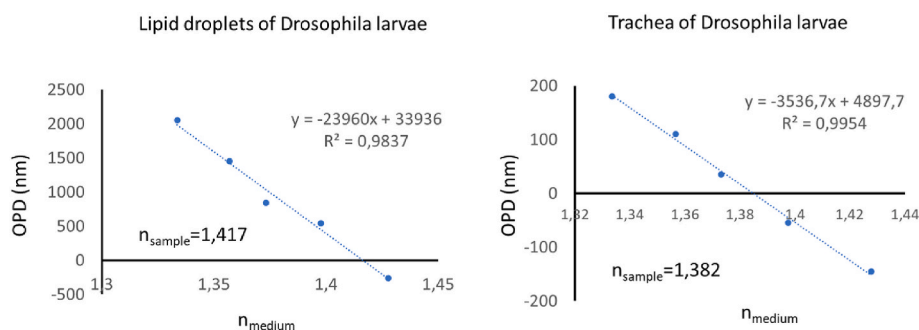
Fig. 10. Estimated RI and thickness from lipid droplets and trachea of *Drosophila* larvae. Left figure indicates a value of average RI of 1417 and an average thickness of 23,9 μm for lipid droplets. Right figure shows an estimated RI of 1382 and an average thickness of 3.54 μm for tracheae.

Table 1
Immersion liquids recommended sets.

Type	Refractive index range	Samples	Components/ Refractive index(D20)
Oils	1,42-1,65	Inorganic -Hydrophobic Low density solids	Silicone oil - 1,403 Coconut oil - 1,461 Paraffin oil - 1,473 Castor oil - 1,478 Cedar oil – 1,510 Immersion oil – 1,516 Anise oil – 1,561 Cassia oil – 1,605
Alcohols	1,328-1,418	Inorganic samples Organic samples	Methanol – 1,328 Ethanol – 1,362 Propanol – 1,384 Butanol – 1,397 Hexanol – 1,418
Glycerol/ Water	1,333-1,472	Inorganic samples Hydrophilic samples	Water – 1,333 Glycerol – 1,472
Iodixanol/ Water	1,333-1,429	Organic/Biological samples	Water – 1,333 OptiPrep (60% w/v) – 1,429

immersion media methods might reduce the phase artifacts, reduce the background noise and yields more accurate RI.

There are several possible sources of errors in QPI that have been sufficiently reviewed in the literature [37,38]. Ideally, when developing a method such as this, an attempt is made to ensure that the error of the method does not exceed the measurement error of the instrumentation. By increasing the number of solutions with different RIs, the systematic error of the method arising from the immersion liquid preparation will decrease. The phase that naturally produces an immersion liquid, commonly mistaken for instrumentation noise or dust interferences, deserves a further discussion. This phase appears as low frequency features in the image, due to surface liquid undulations, heterogeneous concentrations, diffusion movements, etc., and will largely depend on its physicochemical properties. A carefully study of the cross-section profiles would minimize this issue, although complicates the computational treatment of the method and the task of setting a threshold for extracting the OPD heights. It is advisable to work with pure immersion media, whenever circumstances allow to, or to validate calibration solutions very accurately.

4. Conclusions

The RI in heterogeneous materials reflects an effective value of the volume of sample covered by the beam of light. Besides, the information about the spatial distribution of RI components greatly depends on the technique chosen to measure it. QPI yields 2D distribution of the RI allowing 3D projections of thickness or RI only if the shape of the sample is known. Diffraction-limited resolution achieved for most of the available QPI methods might be enough to study refractive index 2D distribution of single cell organelles of most vegetal and animal cells. The magnitude measured in QPI is an effective difference in the path that travels the light between 2 media of different RI. This magnitude, named OPD, is proportional to both, RI differences of both medium (Δn) and the thickness of the sample. To determine RI by QPI we need to solve this problem but having previous knowledge of the thickness sample or applying any experimental procedure to solve this ambiguity.

Here, we propose a method that uses different immersion media with a well-known RI and distributed in a range that should ideally be close to the unknown RI of the tested sample. This method can be applied to inorganic and biological materials and estimates RI for selected regions of the images that have recurring shape characteristics. We applied the method to a calibration phase target and a microlens array for validation, and we then use it successfully to study the refractive indices of complex biological samples such as onion epidermis cells and lipid droplets/tracheal system in *Drosophila* larvae.

New microscopic techniques offer novel possibilities to redefine concepts as the RI by using new data. As stated in Majeed et al. [39] *"Expressions such as "the RI of the liver is" … does not carry any significant meaning. The RI is a statistical quantity that is best described trough moments (mean, variance, etc.) and spatial correlations"*. In this sense, QPI techniques and simple methods such as the one presented here might help to assign a new definition of RI in heterogeneous materials. Moreover, prospective studies as the one presented in this work will trigger future research exploring the capabilities of QPI to follow the RI evolution in cell dynamics and biological reactions, combined with tomographic techniques, yielding a real 3D distribution with better resolution. This will represent a great step towards the understanding of the crucial role played by cell internal composition changes in biological processes.

Declaration of competing interest

The authors declare that they have no known competing financial interests or personal relationships that could have appeared to influence the work reported in this paper.

Data availability

Data will be made available on request.

Acknowledgements

References

[1] R. Khan, B. Gul, S. Khan, H. Nisar, I. Ahmad, Refractive index of biological tissues: review, measurement techniques, and applications, Photodiagnosis Photodyn. Ther. 33 (2021), https://doi.org/10.1016/j.pdpdt.2021.102192.

[2] Shyam Singh, Refractive index measurement and its applications, Phys. Scripta 65 (2002) 167, https://doi.org/10.1238/Physica.Regular.065a00167.

[3] J. Lai, Z. Li, C. Wang, A. He, Experimental measurement of the refractive index of biological tissues by total internal reflection, in: Appl. Opt., 2005, pp. 1845–1849, https://doi.org/10.1364/AO.44.001845.

[4] R.A. Paselk, The evolution of the abbe refractometer, Bull. Instrum. Soc. (1999) 19–22.

[5] J.-C. Lai, Y.-Y. Zhang, Z.-H. Li, H.-J. Jiang, A.-Z. He, Complex refractive index measurement of biological tissues by attenuated total reflection ellipsometry, Appl. Opt. 49 (2010) 3235–3238, https://doi.org/10.1364/AO.49.003235.

[6] A. Nahmad-Rohen, H. Contreras-Tello, G. Morales-Luna, A. García-Valenzuela, On the effective refractive index of blood, Phys. Scripta 91 (2015), 15503.

[7] J. Lai, Z. Li, C. Wang, A. He, Effective refractive indices of biological tissues and its experimental determination, in: Prog. Biomed. Opt. Imaging - Proc. SPIE, 2005, pp. 558–562, https://doi.org/10.1117/12.571717.

[8] R. Khan, B. Gul, S. Khan, H. Nisar, I. Ahmad, Refractive index of biological tissues: review, measurement techniques, and applications, Photodiagnosis Photodyn. Ther. 33 (2021), https://doi.org/10.1016/j.pdpdt.2021.102192.

[9] S.L. Jacques, Optical properties of biological tissues: a review, Phys. Med. Biol. 58 (2013) R37.

[10] Y.K. Park, C. Depeursinge, G. Popescu, Quantitative phase imaging in biomedicine, Nat. Photonics 12 (2018) 578–589, https://doi.org/10.1038/s41566-018-0253-x.

[11] D. Paganin, K.A. Nugent, Noninterferometric phase determination. https://doi.org/10.1016/S1076-5670(01)80104-X, 2001.

[12] C. Zuo, J. Li, J. Sun, Y. Fan, J. Zhang, L. Lu, R. Zhang, B. Wang, L. Huang, Q. Chen, Transport of intensity equation: a tutorial, Opt Laser. Eng. 135 (2020), https://doi.org/10.1016/j.optlaseng.2020.106187.

[13] G. Popescu, Quantitative Phase Imaging of Cells and Tissues, 2011.

[14] P. Marquet, C. Depeursinge, P.J. Magistretti, Review of quantitative phase-digital holographic microscopy: promising novel imaging technique to resolve neuronal network activity and identify cellular biomarkers of psychiatric disorders, Neurophotonics 1 (2014), 020901, https://doi.org/10.1117/1.nph.1.2.020901.

[15] Y. Ansong, The promise of quantitative phase imaging and machine learning in medical diagnostics: a review, J. Med. Artif. Intell. 3 (2020) 63–65, https://doi.org/10.21037/jmai.2019.10.05.

[16] R.C. Faust, The determination of the refractive indices of inhomogeneous solids by interference microscopy, Proc. Phys. Soc. B 67 (1954) 138, https://doi.org/10.1088/0370-1301/67/2/306.

[17] J. Song, J. Min, X. Yuan, Y. Xue, C. Bai, B. Yao, Triple-wavelength quantitative phase imaging with refractive index measurement, Opt Laser. Eng. 156 (2022), https://doi.org/10.1016/j.optlaseng.2022.107110.

[18] H. Park, T. Ahn, K. Kim, S. Lee, S. Kook, D. Lee, I.B. Suh, S. Na, Y. Park, 3-D Refractive Index Tomograms and Deformability of Individual Human Red Blood Cells from Cord Blood of Newborn Infants and Maternal Blood, (n.d)..

[19] H. Tang, X. Liu, S. Chen, X. Yu, Y. Luo, J. Wu, X. Wang, L. Liu, Estimation of refractive index for biological tissue using micro-optical coherence tomography, IEEE Trans. Biomed. Eng. 66 (2019) 1803–1809, https://doi.org/10.1109/TBME.2018.2885844.

[20] H. Yagoda, Physical techniques in biological research, in: Gerald Oster, Arthur W. Pollister (Eds.), Optical Techniques, 123, Academic Press, New York, 1956, p. 741, 1955. xiii+ 564 pp. Illus. $13.50., Science (80-.).

[21] T. Kitazawa, T. Nomura, Refractive index tomography based on optical coherence tomography and tomographic reconstruction algorithm, Jpn. J. Appl. Phys. 56 (2017), 09NB03.

[22] P. Marquet, E. Bélanger, É. Rioux-Pellerin, P. Lavergne, B. de Dorlodot, S. A. Lévesque, P. Jourdain, P. Magistretti, Exploring living neuronal network dynamics and homeostasis with multimodal digital holographic microscopy: towards identifying early biomarkers for neurodevelopmental disorders, in: Digit. Hologr. Three-Dimensional Imaging 2019, Optical Society of America, Bordeaux, 2019. Th1A.3, http://www.osapublishing.org/abstract.cfm?URI=DH-2019-Th1A.3.

[23] R.C. Faust, The determination of the refractive indices of inhomogeneous solids by interference microscopy, Proc. Phys. Soc. B 67 (1954) 138, https://doi.org/10.1088/0370-1301/67/2/306.

[24] H. Tang, X. Liu, S. Chen, X. Yu, Y. Luo, J. Wu, X. Wang, L. Liu, Estimation of refractive index for biological tissue using micro-optical coherence tomography, IEEE Trans. Biomed. Eng. 66 (2019) 1803–1809, https://doi.org/10.1109/TBME.2018.2885844.

[25] J.M. Trujillo-Sevilla, M. Velasco-Ocaña, S. Bonaque-González, C. Belda-Para, J. M. Rodríguez-Ramos, Wavefront phase measurement of striae in optical glass, Appl. Opt. 61 (2022) 3912, https://doi.org/10.1364/ao.450219.

[26] S. Bonaque-González, J.M. Trujillo-Sevilla, M. Velasco-Ocaña, Ó. Casanova-González, M. Sicilia-Cabrera, A. Roqué-Velasco, S. Ceruso, R. Oliva-García, J. Martín-Hernández, O. Gomez-Cardenes, J.G. Marichal-Hernández, D. Gatinel, J. T. Holladay, J.M. Rodríguez-Ramos, The optics of the human eye at 8.6 µm resolution, Sci. Rep. 11 (2021), 23334, https://doi.org/10.1038/s41598-021-02653-w.

[27] C. Zuo, J. Li, J. Sun, Y. Fan, J. Zhang, L. Lu, R. Zhang, B. Wang, L. Huang, Q. Chen, Transport of intensity equation: a tutorial, Opt Laser. Eng. 135 (2020), 106187, https://doi.org/10.1016/j.optlaseng.2020.106187.

[28] A. Abou Khalil, W. Gebremichael, Y. Petit, L. Canioni, Refractive index change measurement by quantitative microscopy phase imaging for femtosecond laser written structures, Opt Commun. 485 (2021), 126731, https://doi.org/10.1016/j.optcom.2020.126731.

[29] E. Belanger, S.A. Levesque, E. Rioux-Pellerin, J.-M. Mugnes, V. Watters, V. Roy, A. Bernatchez, G. Anctil, P. Marquet, Solving the refractive index - thickness ambiguity in quantitative phase imaging of primary neurons in culture with a low-cost custom-made 3D-printed perfusion chamber, in: Opt. InfoBase Conf. Pap., 2018, https://doi.org/10.1364/TRANSLATIONAL.2018.JTu3A.16.

[30] T. Boothe, L. Hilbert, M. Heide, L. Berninger, W.B. Huttner, V. Zaburdaev, N. L. Vastenhouw, E.W. Myers, D.N. Drechsel, J.C. Rink, A tunable refractive index matching medium for live imaging cells, tissues and model organisms, Elife 6 (2017) 1–15, https://doi.org/10.7554/eLife.27240.

[31] P.O. Larsson, N. Leiva Eriksson, Seeing through cells: rapid measurement of intracellular target proteins, Front. Bioeng. Biotechnol. 10 (2022), https://doi.org/10.3389/fbioe.2022.996224.

[32] K. Kafle, X. Xi, C.M. Lee, B.R. Tittmann, D.J. Cosgrove, Y.B. Park, S.H. Kim, Cellulose microfibril orientation in onion (Allium cepa L.) epidermis studied by atomic force microscopy (AFM) and vibrational sum frequency generation (SFG) spectroscopy, Cellulose 21 (2014) 1075–1086.

[33] Z. Wang, V. Bianco, D. Pirone, P. Memmolo, M.M. Villone, P.L. Maffettone, P. Ferraro, Dehydration of plant cells shoves nuclei rotation allowing for 3D phase-contrast tomography, Light Sci. Appl. 10 (2021), https://doi.org/10.1038/s41377-021-00626-2.

[34] C.A. Peterson, R.L. Peterson, A.W. Robards, A correlated histochemical and ultrastructural study of the epidermis and hypodermis of onion roots, Protoplasma 96 (1978) 1–21, https://doi.org/10.1007/BF01279571.

[35] S. Natonik-Białoń, D. Borowska-Wykręt, G. Mosca, M. Grelowski, R. Wrzalik, R. S. Smith, D. Kwiatkowska, Deformation of a cell monolayer due to osmotic treatment: a case study of onion scale epidermis, Botany 98 (2020) 21–36, https://doi.org/10.1139/cjb-2019-0027.

[36] L. Renhua, P. Michael, O. Brian, Lipid profiles of female and male Drosophila, in: BMC, 2011.

[37] M. Bedrossian, J. Nadeau, E. Serabyn, C. Lindensmith, Sources and propagation of errors in quantitative phase imaging techniques using optical interferometry, in: Quant. Phase Imaging III, SPIE, 2017, pp. 6–16.

[38] T.L. Nguyen, S. Pradeep, R.L. Judson-Torres, J. Reed, M.A. Teitell, T.A. Zangle, Quantitative phase imaging: recent advances and expanding potential in biomedicine, ACS Nano 16 (2022) 11516–11544.

[39] H. Majeed, S. Sridharan, M. Mir, L. Ma, E. Min, W. Jung, G. Popescu, Quantitative phase imaging for medical diagnosis, J. Biophot. 10 (2017) 177–205, https://doi.org/10.1002/jbio.201600113.